Bioorganic & Medicinal Chemistry Letters 26 (2016) 1011–1015

Contents lists available at ScienceDirect

Bioorganic & Medicinal Chemistry Letters

journal homepage: www.elsevier.com/locate/bmcl

Three-dimensional QSAR analysis and design of new 1,2,4-oxadiazole antibacterials

Erika Leemans [†], Kiran V. Mahasenan [†], Malika Kumarasiri, Edward Spink, Derong Ding, Peter I. O'Daniel, Marc A. Boudreau, Elena Lastochkin, Sebastian A. Testero, Takao Yamaguchi, Mijoon Lee, Dusan Hesek, Jed F. Fisher, Mayland Chang, Shahriar Mobashery *

Department of Chemistry and Biochemistry, University of Notre Dame, Notre Dame, IN 46556, USA

ARTICLE INFO

Article history:
Received 30 October 2015
Accepted 11 December 2015
Available online 12 December 2015

Keywords:
1,2,4-Oxadiazole
Antibiotic
3D-QSAR
CoMFA

ABSTRACT

The oxadiazole antibacterials, a class of newly discovered compounds that are active against Gram-positive bacteria, target bacterial cell-wall biosynthesis by inhibition of a family of essential enzymes, the penicillin-binding proteins. Ligand-based 3D-QSAR analyses by comparative molecular field analysis (CoMFA), comparative molecular shape indices analysis (CoMSIA) and Field-Based 3D-QSAR evaluated a series of 102 members of this class. This series included inactive compounds as well as compounds that were moderately to strongly antibacterial against *Staphylococcus aureus*. Multiple models were constructed using different types of energy minimization and charge calculations. CoMFA derived contour maps successfully defined favored and disfavored regions of the molecules in terms of steric and electrostatic properties for substitution.

The profligate use of antibiotics has accelerated not just the evolution of antibiotic resistance, but also the epidemiological landscape, of both the Gram-positive and Gram-negative bacteria. Among the many examples of this transformation is the transition of the β-lactam antibiotic-resistant Gram-positive pathogen *Staphylococcus aureus* from the hospital into the community.[1–4] The breadth and the rapidity of this transformation (and others like it) have been suggested to correspond to the dawn of a post-antibiotic era.[5] This credible—and no less fearful—prospect has engendered numerous strategic proposals to push back this dawn,[6–10] including especially the importance of the discovery of new antibacterial structure[11,12] and the provision of new economic incentives to revitalize commercial antibacterial development.[13–15] Here, we provide an overview of our extensive effort to systematically probe the structure–activity relationship of a new class of 1,2,4-oxadiazole antibacterials with unprecedented anti-Gram positive activity.

Through computational docking and scoring procedures carried out in our laboratory, we discovered the class of 1,2,4-oxadiazole antibiotics active against Gram-positive bacteria, including *S. aureus*.[16] This antibiotic class inhibits bacterial cell-wall biosynthesis by targeting the function of the penicillin-binding proteins (PBPs). The lead compound (**1**, Fig. 1A) was the basis for extensive structure–activity analysis.[17,18] Here, we use the results of this effort to build a three-dimensional quantitative structure–activity relationship (3D-QSAR) model for these compounds in order to assist the design of novel analogs with improved activity.

The 3D-QSAR methods rely on the principle that the three-dimensional geometric and electronic features of molecules correlate with their biological activities.[19] 3D-QSAR plays an important role in the optimization of pharmacologically active compounds and in the prediction of the biological activity of newly synthesized compounds.[20] Cramer has elegantly captured the reasons behind a QSAR renaissance for ligand-based design.[21] Comparative molecular field analysis (CoMFA)[22] aligns molecules in a three-dimensional lattice and calculates their steric (Lennard–Jones potential) and electrostatic (Coulomb potential) molecular descriptors. These CoMFA descriptors can be used to build a partial least squares (PLS) statistical model that correlates the molecular structures with the biological activity. Comparative molecular shape indices analysis (CoMSIA) incorporates hydrophobic and hydrogen-bond donor/acceptor descriptors in addition to steric and electrostatic descrip-

Abbreviations: CoMFA, comparative molecular field analysis; CoMSIA, comparative molecular shape indices analysis; GH, Gasteiger–Hückel; LOO, leave-one-out method; MIC, minimum inhibitory concentration; MM, molecular mechanics; MMFF94, Merck Molecular Force Field 94; PLS, partial least squares; QM, quantum mechanical; SEE, standard error of estimate.

* Corresponding author. Tel.: +1 574 631 2933; fax: +1 574 631 6652.
E-mail address: mobashery@nd.edu (S. Mobashery).

† The first two authors contributed equally.

http://dx.doi.org/10.1016/j.bmcl.2015.12.041
0960-894X/

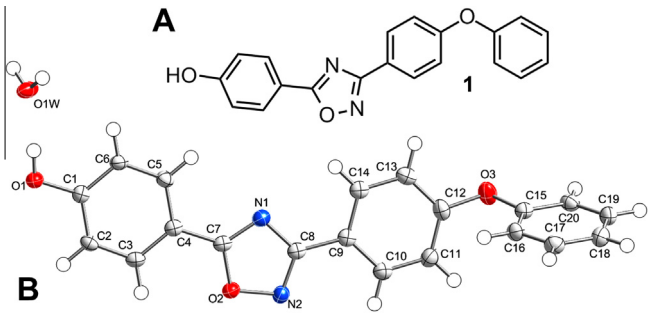

Figure 1. (A) Chemical structure of antibiotic **1**; (B) the ORTEP structure for the crystal structure of **1** shown at 50% probability level. H atoms are shown as spheres of arbitrary radii.

tors. Contour maps obtained from CoMFA calculations identified favored and disfavored regions of the lead oxadiazole compound in terms of steric and electrostatic properties for further lead optimization. Based on the investigation, recommendations for the design of new oxadiazole analogs are proposed.

The performance of the standard CoMFA and CoMSIA procedures requires the specification of both the conformations and alignments of the molecules. All of our structures were superimposed onto the X-ray crystal structure of **1** (Fig. 1B). Selection of appropriate and accurate methods to assign partial charges of each atom in a molecule is a critical step in QSAR study. Energy minimization with different charge methods is required to create robust CoMFA and CoMSIA models.[23] Molecular mechanics (MM) methods are most commonly used to derive molecular charges for CoMFA and CoMSIA calculations. We first used the standard Tripos Molecular Mechanics force field to determine the Gasteiger–Hückel charges. Our second method applied the Powell method via the Merck Molecular Force Field and added MMFF94 charges to the molecular dataset.[24] This method has been given increasing attention as a more accurate general-use empirical partial charge method.[23] In order to further improve the accuracy, a third method used quantum–mechanical charge calculation to introduce restrained electrostatic potential (RESP) charges.[25] The molecular alignments for the compounds that were energy minimized containing Gasteiger–Hückel and QM charges are shown from two different viewpoints (Fig. S2 in the Supporting information). Additionally, Field-Based QSAR, a 3D-QSAR method developed by Schrödinger Inc., was also used.

The dataset of 102 synthetic oxadiazoles was randomly divided into a training set of 77 compounds and a test set of 25 compounds (see Fig. 2 for a representative set of compound structures and Table S1 in the Supporting information for full set of compounds). Both sets represent equally well the chemical and biological properties of the entire data set, as per recommendations of Golbraikh et al.[26] The measurement of antibacterial activity was expressed as *p*MIC (*p*MIC = $-\log_e$(MIC/MW), where the MIC values were experimental ones determined against *S. aureus*. The compounds in our data set represent an activity range of greater than five log units, from a minimum *p*MIC of 0.63 (least active) to a maximum *p*MIC of 7.4 (most active). Data analysis by PLS regression linearly correlated CoMFA and CoMSIA values with the calculated field descriptors as independent variables and the *p*MIC values as dependent variables.[22]

The dataset with Gasteiger–Hückel charges was first analyzed by CoMFA. The training set provided a cross-validation correlation coefficient q^2 of 0.52 with the leave-one-out method (LOO) to evaluate internal predictive quality.[27,28] A non-validated r^2 value of 0.82 was obtained using five components (see Table 1), thus demonstrating a satisfactory level of internal predicting power.[29] However, Golbraikh and Tropsha state that q^2 alone is not sufficient for reliable predictive power. The only way of validating predictive power reliably is by the use of an external test set.[27,29,30] The activity values for the predictive compounds (the test set) gave an r^2_{pred} of 0.55, thus indicating a reasonable predictive power of the model. This predicted r^2 assesses the robustness of the QSAR model. A graph of the experimental versus the residual values showed that the residual values were mostly lower than the standard error of estimate (SEE) of 0.90, as a measure of the accuracy of the predictions (see Fig. S3-B in the Supporting information).

3D-QSAR CoMFA analysis of the data set with empirical MMFF94 charges was generated in an identical manner. The cross-validated q^2 value of 0.70 for the same training set improved in comparison to the one obtained with Gasteiger–Hückel charges ($q^2 = 0.52$), whereas the non-validated r^2 value (0.85) was in the same range. Analyzing the test set by the model gave a much higher r^2_{pred} of 0.77 (see Table 1, and Fig. S4 in the Supporting information).

More complex ab initio quantum–mechanical charge calculations were carried out in an effort toward improvement of the accuracy to describe molecular interactions. The RESP method (ab initio energy minimization of structures at the Hartree–Fock level, using the 6-31G(d) basic set) was used to determine the electrostatic charges. Gaussian 09 performed these calculations, and the antechamber module of Amber 12 applied the derived RESP changes. The internal cross-validation q^2 (0.52) and the non-validated r^2 value (0.88) were similar to those with the empirical Gasteiger–Hückel charges ($q^2 = 0.52$, $r^2 = 0.88$). Validation using the test set of 25 compounds gave an acceptable r^2_{pred} value of 0.61 (see Table 1 and Fig. S5 in the Supporting information).

Based on previous reports that the inclusion of hydrophobic properties could improve a QSAR model, the value of including Log*P* as an added descriptor was assessed.[31] When *c*Log*P* (CambridgeSoft ChemBioDraw Ultra 2010, 12.0) was introduced as a lipophilicity molecular descriptor, the model carrying Gasteiger–Hückel charges improved slightly from a q^2 value of 0.52 and an r^2 value of 0.82 to a q^2 of 0.55 and an r^2 of 0.83, respectively (see Table 1). However, the r^2_{pred} value of the test set decreased from 0.55 to 0.31. For the model with MMFF94 charges, adding *c*Log*P* as an extra descriptor gave an inconsequential improvement for q^2 (from 0.70 to 0.71). At the same time, r^2_{pred} value decreased drastically from 0.77 to 0.44 for the test set, indicating reduced predictive ability. For the model using QM charges and *c*Log*P*, the q^2 and r^2 values improved to 0.60 and 0.89 in comparison to 0.52 and 0.88, respectively. The r^2_{pred} value of 0.56 was slightly lower than that for the model without the use of *c*Log*P* (0.61). The models with *c*Log*P* required additional PLS components. Cramer and Wendt indicate that small improvements of q^2 as a result of incorporating *c*Log*P* is offset by the increase in PLS components.[30] These results indicated that the addition of a *c*Log*P* descriptor did not give improved models.

We applied a second method, CoMSIA, which incorporates hydrophobic and hydrogen-bond donor/acceptor features in addition to steric and electrostatic descriptors. For the CoMSIA method with Gasteiger–Hückel charge calculation, better results were achieved in comparison with CoMFA. However, this model required additional PLS components. The CoMSIA analysis for the same training and test sets using MMFF94 charges ($q^2 = 0.66$, $r^2 = 0.90$; $n = 6$) gave comparable results to the CoMFA analysis ($q^2 = 0.70$, $r^2 = 0.85$; $n = 5$). The predicted r^2 for CoMSIA was lower ($r^2_{pred} = 0.58$) than the one obtained with CoMFA ($r^2_{pred} = 0.77$), indicating that CoMFA had more predictive ability. The quantum–mechanical results for the CoMSIA analysis produced less satisfactory results in comparison to CoMFA.

Field-Based QSAR (Schrödinger Inc.) is a 3D-QSAR approach similar to CoMFA/CoMSIA but uses different parameters.[32] In the

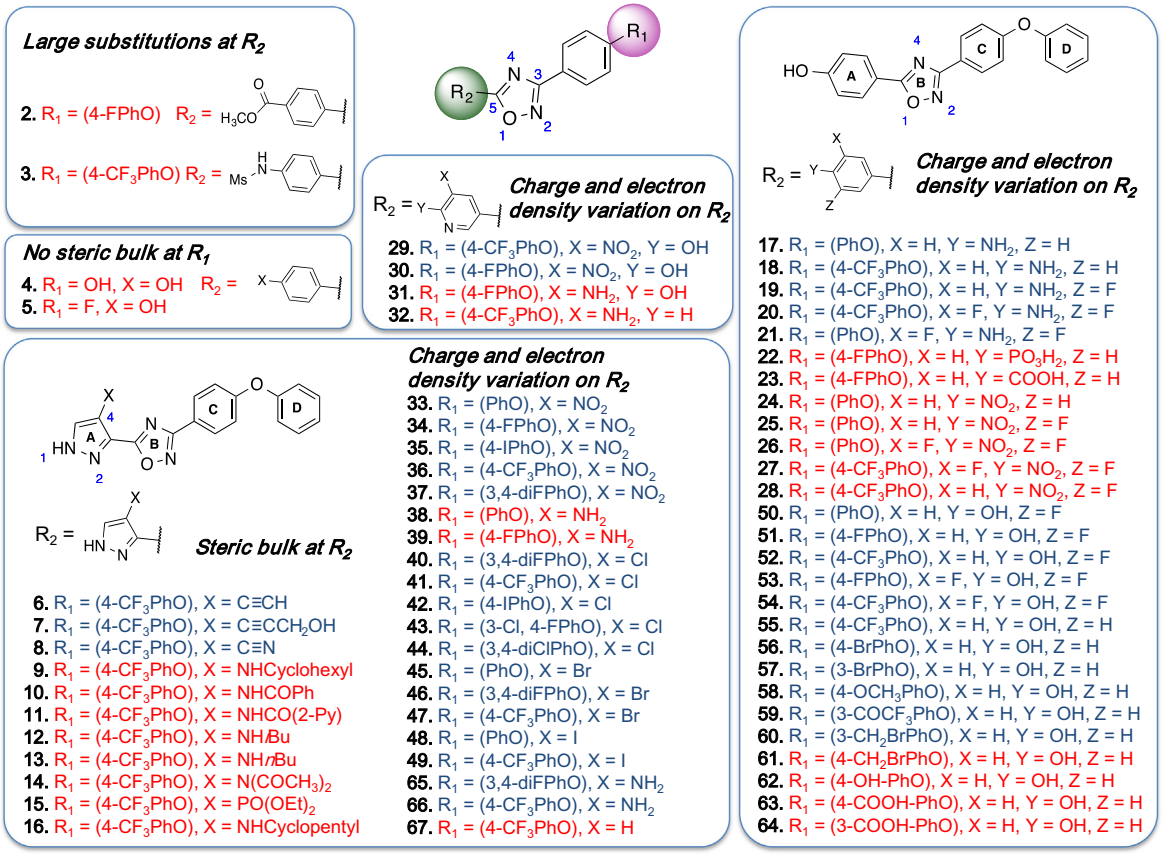

Figure 2. Representative 1,2,4-oxadiazole structures of the 102 compound set, demonstrating the molecular diversity used in the analyses. Compound activity was assessed by MIC determinations against a standard, methicillin-sensitive strain of *S. aureus* (ATCC 29213). Active compounds (MIC ⩽ 8 μg/ml) are in blue letters, while inactives (MIC > 8 μg/ml) are in red letters. The *p*MIC value of **1** is 5.8. This figure includes all of the compounds more active than **1**. These compounds are **6** (*p*MIC = 7.4, the most active compound of the entire series), **18**, **34**, **40**, **41**, **42**, **44**, **45**, **46** and **55**. The complete dataset of structures and biological activity is given as Table S1 of the Supporting information.

Table 1
Statistical results for CoMFA, CoMFA + cLog*P*, CoMSIA and Field-Based QSAR

	CoMFA			CoMFA + *c*Log*P*			CoMSIA			Field-Based QSAR					
										Force field			Gaussian		
Charge calculation	GH	MMFF94	QM	GH	MMFF94	QM	GH	MMFF94	QM	GH	MMFF94	QM	GH	MMFF94	QM
Values															
q^2[a]	0.52	0.70	0.52	0.55	0.71	0.60	0.63	0.66	0.46	0.64	0.68	0.32	0.55	0.61	0.47
r^2	0.82	0.85	0.88	0.83	0.85	0.89	0.90	0.90	0.75	0.91	0.92	0.73	0.88	0.90	0.72
SEE[b]	0.90	0.84	0.72	0.88	0.82	0.71	0.70	0.69	1.01	0.64	0.62	1.05	0.75	0.86	1.06
n[c]	5	5	6	6	6	7	7	6	3	6	6	4	7	5	3
F-test	66.2	77.6	74.8	57.8	68.3	66.3	83.9	103.5	65.2	120.5	130.3	43.4	72.1	73.1	56.1
r^2_{pred}	0.55	0.77	0.61	0.31	0.44	0.56	0.61	0.58	0.39	0.68	0.74	0.14	0.68	0.69	0.22
Field distribution %															
Steric	35.6	37.1	39.9	35.0	35.0	37.4	6.6	7.6	8.5	34.1	33.1	40.0	32.0	35.4	36.2
Electro-static	64.4	62.9	60.1	60.2	59.6	58.4	32.0	34.4	33.4	65.9	67.9	60.0	13.2	12.5	9.2
*c*Log*P*				4.8	4.5	4.2									
Hydrophobic							16.3	13.7	10.7				15.5	13.5	20.2
Donor							26.5	26.5	32.6				23.4	24.9	16.8
Acceptor							17.4	17.9	14.8				15.9	13.6	17.7

[a] q^2 from the leave-one-out.
[b] Standard error of estimate.
[c] Optimum number of components.

force-field method of this approach, the ligands were given Lennard–Jones steric potentials from OPLS2005 force field and previously calculated atomic charges for the electrostatic properties. For the Gaussian method, molecular hydrophobicity was determined according to Ghose et al. via ALOGP and CLOGP methods.[33] Hydrogen-bond donor and hydrogen-bond acceptor pharmacophore features were provided by PHASE. The CoMFA and CoMSIA models with Gasteiger–Hückel and MMFF94 charges were compared to force field and Gaussian methods, respectively. As seen in Table 1, the MMFF94 charge calculations provided the best

model for the force field as well as for the Gaussian method with q^2 values of 0.68 and 0.61, non-validated r^2 of 0.92 and 0.90, and r^2_{pred} of 0.74 and 0.69, respectively. The model carrying Gasteiger–Hückel charges also resulted in good values for both the force field ($q^2 = 0.64$, $r^2 = 0.91$, $n = 6$) and the Gaussian approach ($q^2 = 0.55$, $r^2 = 0.88$, $n = 7$). Results for models that used quantum–mechanical charges were less satisfactory than the other two models.

The graphic representation of CoMFA contour maps in 3D space was created using the data from the PLS analysis. With these maps, the steric and electrostatic features of the compounds were analyzed. The steric CoMFA map indicates the areas where steric bulk is favored (green contours) or disfavored (yellow contours), as shown in Fig. 3A. The electrostatic contour map is shown in Fig. 3B. The blue polyhedrals represent favorable regions for electropositive substituents, and the red polyhedrals represent favorable regions for electronegative substituents. The two sub-classes of compounds, that is, the 5-phenyl- and 5-(pyrazol-3-yl)-substituted 1,2,4-oxadiazoles, contributing to this model were examined (see Fig. S1).

Compounds in the training set were initially analyzed to identify the features of the antibiotic activity in relation to the maps. For the 5-phenyl-1,2,4-oxadiazoles, large substitutions at the *para*-position of the phenyl ring are not tolerated, as indicated by the yellow contour. For example, both **2** (*p*-CO_2Me) and **3** (*p*-$NHSO_2$Me) are inactive. This map also suggests that a steric feature is favored at the 3-phenoxyphenyl group of the 1,2,4-oxadiazole (R_1 position), as shown by the green contour. This conclusion is supported by the inactive compounds that lack this ring (**4**, and **5**). The small green contour at position 4 of the 5-(pyrazol-3-yl)-1,2,4-oxadiazoles indicates that steric substitutions are preferred close to that region, as exemplified by the iodo-substituted active compounds **48** and **49**. However, further increasing the bulk at the same position, and thus extending substitutions to the steric-disfavored yellow map region in the vicinity, is proposed to be detrimental to the activity. This suggestion by the model is corroborated by inactive compounds with bulkier substitutions (**9**, **10**, **11**, **12**, **13**, and **14**).

Furthermore, electrostatic features were visualized by blue and red contours, which indicate favorable electropositive and electronegative groups, respectively (Fig. 3B). When 5-phenyl-1,2,4-oxadiazoles were analyzed, a blue contour was observed close to the *para*-position of the phenyl ring, which recommends positively charged substitutions to enhance antibacterial activity. 5-(4-Aminophenyl)-1,2,4-oxadiazoles (**17**, **18**, **19**, **20**, and **21**) follow this trend. Accordingly, compounds **22**, **23**, **24**, **25**, **26**, and **27**, which carry high partial negative charge in this region, are inactive. At the *ortho*- and *meta*-positions of the phenyl ring, red contours indicate that increased electron density improves activity. Therefore, compounds with higher electron density like *meta*-NO_2 (**29** and **30**) are active, while substitution with *meta*-NH_2 group make **31** inactive. Similarly, for 5-(pyrazol-3-yl)-1,2,4-oxadiazoles, substitution with NO_2 group is favored at the 4-position of the pyrazole ring, and thus the compounds **33**, **34**, **35**, and **36** are active. Replacing NO_2 group with NH_2 (compounds **38** and **39**) is detrimental to the activity, thus demonstrating unfavorable positive charge at this position.

Analysis of the compounds in the test set reveal that the features of the map correlated well with their respective activities. Acetylene functionality of 4-acetylene-substituted 5-(pyrazol-3-yl)-1,2,4-oxadiazole **6** favorably occupies the small steric map region and shows good activity. Active compounds **7** and **8** also fit well in the steric-favored contour map. At the same time, compounds with bulkier diethyl phosphonate (**15**) and cyclopentane (**16**) substitution in this region extends to the steric disfavored yellow contour map and were inactive. Compound **37** with nitro substitution at this position was active, as supported by the red

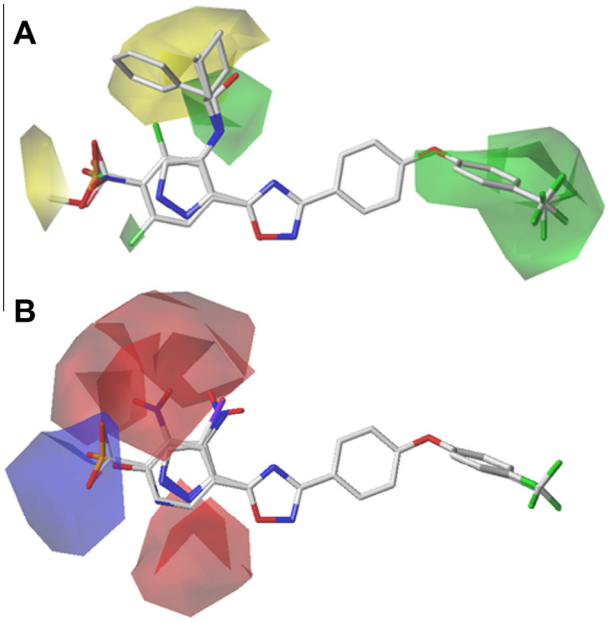

Figure 3. (A) CoMFA steric contour maps: green contours represent steric-bulk-favored region and yellow contours show steric-disfavored position. (B) CoMFA electrostatic contour maps: blue maps display favorable regions for electropositive substituents, while the red polyhedrals show favorable regions for electronegative substituents. The generation of a single map encompassing the phenyl- and pyrazolyl-substituted oxadiazoles (superimposed at the far left) supports the selection of the pyrazolyl rotamer that is shown in this figure as the biologically active conformation.

contour map in the vicinity. As just noted, the positively charged amine substitution of compound **38** is against the recommendation made by the maps, and results in loss of activity. The 5-phenyl-1,2,4-oxadiazole derivative **28** with the nitro substitution at the *para* position of the phenyl ring (ring A) was inactive. Our model recommends positive charge at this position. Electropositive amine substitution at the *meta*-positions of the phenyl ring renders **32** inactive.

Analogous steric and electrostatic contour maps for CoMSIA were generated (shown in Figs. S7A and S7B in the Supporting Information). The CoMSIA hydrophobic contour map (Fig. S7E) revealed hydrophilic preference around the 5-phenyl and 5-(pyrazol-3-yl) ring of the 1,2,4-oxadiazole for increasing activity. Indeed, compounds like **9**, **12**, **13**, and **16** have hydrophobic groups in this region, and they are inactive. However, the hydrophobic contour map at the 3-phenoxyphenyl region did not correlate with the activity of the compounds. Similarly, hydrogen-bond donor/acceptor maps (see Figs. S7C and S7D) failed to provide a satisfactory explanation of the activities.

Supported by these analyses, we formulated guidelines toward the synthesis of analogs of 5-phenyl- and 5-(pyrazol-3-yl)-substituted 1,2,4-oxadiazoles with improved biological activity. The CoMFA steric and electrostatic contour maps of the model generated with MMFF94 charges were used to identify different regions on the molecular template, where any changes could alter the biological activity of the compounds. At the 3-position of the 3-phenyl-1,2,4-oxadiazole (R_1), a bulky *para*-substituent is favorable for the activity, as indicated by the steric contour map. Compounds with small substituents like hydroxyl (**4**) or fluoride (**5**) at this position are inactive. An aromatic ring at this position (ring D, see Fig. 2) appears to be critical for activity. Activity is mostly retained by substitution of F, Cl, I and CF_3 at the *meta*- or *para*-positions of this phenyl ring of the 4-chloro (**40**, **41**, **42**, **43** and **44**), 4-bromo (**45**, **46**, and **47**), and 4-iodo (**48** and **49**) (pyrazol-3-yl)-

1,2,4-oxadiazoles. A similar observation can be made for 5-phenyl-1,2,4-oxadiazoles **50**, **51**, **52**, **53**, **54**, and **55**. In addition, compounds **56** and **57** show that *meta*- or *para*-bromo substitutions were also acceptable. CoMFA green contour map towards the *meta*- and *para*-position suggest that bulkier groups can be accommodated at this region. This is exemplified by methoxy (**58**), trifluoroacetyl (**59**) and *meta*-bromomethyl (**60**) substitutions at this region. However, contrary to this recommendation, *para*-bromomethyl (**61**) analog was inactive. Loss of activity was also observed for hydroxyl (**62**), and carboxylic acid (**63** and **64**) substitutions. CoMFA steric or electrostatic maps were unable to rationalize these activities.

For the 5-phenyl-1,2,4-oxadiazoles, large substitutions at the *para*-position of the phenyl ring (ring A, see Fig. 2) are not tolerated as indicated by compounds **2** and **3**. At the same position, positively charged substitutions like an amine group (**17**, **18**, **19**, **20**, and **21**) are favored by the CoMFA electrostatic map. For the same reason, the nitro group and negatively charged carboxylate at this position (**22**, **23**, **24**, **25**, **26**, and **27**) rendered the compounds inactive. At the *ortho*- and *meta*-positions of the phenyl ring, or at the 3- and 4-positions of the pyrazole ring, the CoMFA electrostatic map recommended negatively charged or electron-dense substitutions. Thus the NO_2-substituted compounds (**29**, **30**, **33**, **34**, **35**, **36** and **37**) were active, while the amino-substituted compounds (**31**, **32**, **38** and **39**) were inactive. However, compounds **65** and **66** did not follow this trend. Bulky substituents like cyclohexyl, cyclopentyl or benzamide at the 4-position of the 5-(pyrazole-3-yl)-1,2,4-oxadiazoles are not favored (**9**, **10**, **11**, **12**, **13**, **14**, **15**, and **16**). On the other hand, smaller substituents are recommended by the maps at the same place. The importance of substitution at this position is exemplified by the unsubstituted compound (**67**), which is inactive compared to chloro-, bromo-, or iodo- substituted analogs (**41**, **47** and **49**, respectively).

A limitation of these calculation is their use of MIC values as the experimental biological descriptor. MIC values represent the sum of separate biological contributors such as penetration through the cell wall or the collective interaction within the many members of the family of penicillin-binding proteins, the target enzymes of these antibiotics. But since PBPs are found at the surface of the outer leaflet of the membrane of Gram-positive bacteria, the compounds need only to diffuse through the cell wall to reach their target. The compounds do not need to pass through the membrane. Diffusion through the cell wall for these small molecules may not be strongly dependent on structure (within this antibiotic class). Similarly, if inhibition of a single PBP (out of the five found in MRSA), for example PBP2a, is the critical biological target, this conclusion is even more reasonable. These observations bolster confidence in the models studied in this Letter as foundational for the future design of more potent antibacterials within this class.

Acknowledgment

This work was supported by the National Institutes of Health (AI90818).

Supplementary data

Supplementary data (ring designation of the 5-phenyl-type and 5-(pyrazol-3-yl)-type 1,2,4-oxadiazoles, chemical structures of all the compounds in the dataset, alignment of MMFF94 and QM charge calculations, the values of *c*Log*P* and MIC, computational experimentals, plots of the experimental versus predicted values for the different models, plots of the experimental versus the residual values, contour maps of CoMSIA analysis, and the conditions used to grow the crystal of compound **1** and to solve its crystal structure) associated with this article can be found, in the online version, at http://dx.doi.org/10.1016/j.bmcl.2015.12.041.

References and notes

1. Deurenberg, R.; Stobberingh, E. *Infect. Genet. Evol.* **2008**, *8*, 747.
2. Moellering, R., Jr. *J. Antimicrob. Chemother.* **2012**, *67*, 4.
3. Otto, M. *Cell. Microbiol.* **2012**, *14*, 1513.
4. Stryjewski, M.; Corey, G. *Clin. Infect. Dis.* **2014**, *58*, S10.
5. Falagas, M.; Bliziotis, I. *Int. J. Antimicrob. Agents* **2007**, *29*, 630.
6. Bush, K. *Curr. Opin. Pharmacol.* **2012**, *12*, 527.
7. Bush, K.; Courvalin, P.; Dantas, G.; Davies, J.; Eisenstein, B.; Huovinen, P.; Jacoby, G.; Kishony, R.; Kreiswirth, B.; Kutter, E.; Lerner, S.; Levy, S.; Lewis, K.; Lomovskaya, O.; Miller, J.; Mobashery, S.; Piddock, L.; Projan, S.; Thomas, C.; Tomasz, A.; Tulkens, P.; Walsh, T.; Watson, J.; Witkowski, J.; Witte, W.; Wright, G.; Yeh, P.; Zgurskaya, H. *Nat. Rev. Microbiol.* **2011**, *9*, 894.
8. Fisher, J.; Johnson, J.; Mobashery, S. In *Handbook of Antimicrobial Resistance*; Götte, M., Berghuis, A., Matlashewski, G., Wainberg, M., Sheppard, D., Eds.; Springer Science + Business Media: New York, 2014. p Chap. 12 (29 pp.).
9. Lewis, K. *Nat. Rev. Drug Discov.* **2013**, *12*, 371.
10. Piddock, L. *Lancet Infect. Dis.* **2012**, *12*, 249.
11. Fischbach, M.; Walsh, C. *Science* **2009**, *325*, 1089.
12. Wright, G. *ACS Infect. Dis.* **2015**, *1*, 80.
13. McKellar, M.; Fendrick, A. *Clin. Infect. Dis.* **2014**, *59*, S104.
14. Metz, M.; Shlaes, D. *Antimicrob. Agents Chemother.* **2014**, *58*, 4253.
15. Verhoef, T.; Morris, S. *Chem. Biol. Drug Des.* **2015**, *85*, 4.
16. O'Daniel, P. I.; Peng, Z.; Pi, H.; Testero, S. A.; Ding, D.; Spink, E.; Leemans, E.; Boudreau, M. A.; Yamaguchi, T.; Schroeder, V. A.; Wolter, W. R.; Llarrull, L. I.; Song, W.; Lastochkin, E.; Kumarasiri, M.; Antunes, N. T.; Espahbodi, M.; Lichtenwalter, K.; Suckow, M. A.; Vakulenko, S.; Mobashery, S.; Chang, M. *J. Am. Chem. Soc.* **2014**, *136*, 3664.
17. Ding, D.; Boudreau, M. A.; Leemans, E.; Spink, E.; Yamaguchi, T.; Testero, S. A.; O'Daniel, P. I.; Lastochkin, E.; Chang, M.; Mobashery, S. *Bioorg. Med. Chem. Lett.* **2015**, *25*, 4854.
18. Spink, E.; Ding, D.; Peng, Z.; Boudreau, M. A.; Leemans, E.; Lastochkin, E.; Song, W.; Lichtenwalter, K.; O'Daniel, P. I.; Testero, S. A.; Pi, H.; Schroeder, V. A.; Wolter, W. R.; Antunes, N. T.; Suckow, M. A.; Vakulenko, S.; Chang, M.; Mobashery, S. *J. Med. Chem.* **2015**, *58*, 1380.
19. Verma, J.; Khedkar, V. M.; Coutinho, E. C. *Curr. Top. Med. Chem.* **2010**, *10*, 95.
20. Kubinyi, H. *Drug Discov. Today* **1997**, *2*, 538.
21. Cramer, R. *J. Comput. Aided Mol. Des.* **2012**, *26*, 35.
22. Cramer, R. D.; Patterson, D. E.; Bunce, J. D. *J. Am. Chem. Soc.* **1988**, *110*, 5959.
23. Mittal, R. R.; Harris, L.; McKinnon, R. A.; Sorich, M. J. *J. Chem. Inf. Model.* **2009**, *49*, 704.
24. Halgren, T. A. *J. Comput. Chem.* **1996**, *17*, 490.
25. Cornell, W. D.; Cieplak, P.; Bayly, C. I.; Kollmann, P. A. *J. Am. Chem. Soc.* **1993**, *115*, 9620.
26. Golbraikh, A.; Shen, M.; Xiao, Z.; Xiao, Y.-D.; Lee, K.-H.; Tropsha, A. *J. Comput. Aided Mol. Des.* **2003**, *17*, 241.
27. Kroemer, R.; Hecht, P.; Guessregen, S.; Liedl, K. *Perspect. Drug Discov. Des.* **1998**, *12–14*, 41.
28. Tropsha, A.; Cho, S. *Perspect. Drug Discov. Des.* **1998**, *12–14*, 57.
29. Golbraikh, A.; Tropsha, A. *J. Mol. Graph. Model.* **2002**, *20*, 269.
30. Cramer, R.; Wendt, B. *J. Comput. Aided Mol. Des.* **2007**, *21*, 23.
31. Zhang, L.; Tsai, K. C.; Du, L. P.; Fang, H.; Li, M. Y.; Xu, W. F. *Curr. Med. Chem.* **2011**, *18*, 923.
32. Dixon, S.; Smondyrev, A.; Knoll, E.; Rao, S.; Shaw, D.; Friesner, R. *J. Comput. Aided Mol. Des.* **2006**, *20*, 647.
33. Ghose, A. K.; Viswanadhan, V. N.; Wendoloski, J. J. *J. Phys. Chem. A* **1998**, *102*, 3762.